Photopolymeric films with highly tunable refractive index modulation for high precision diffractive optics

Alessio Zanutta,[1] Enrico Orselli,[2] Thomas Fäcke,[2] and Andrea Bianco[1,*]

[1]*INAF-Osservatorio Astronomico di Brera, via Bianchi 46, 23807, Merate, Italy*
[2]*Covestro AG, Kaiser-Wilhelm-Allee 60,51373 Leverkusen, Germany*
[*]*andrea.bianco@brera.inaf.it*

Abstract: The design and manufacturing of high efficiency and reliable volume phase holographic optical elements require photosensitive material where it is possible to finely control the refractive index modulation. Bayfol HX photopolymers show this feature together with other interesting advantages, in particular the self-developing and the large refractive index modulation. In this paper, the design of Volume Phase Holographic Gratings (VPHGs) is reported underlying the relationship of gratings' performances with the refractive index modulation. The trend of this property with the change of the laser power density and the ratio of the two writing beams is shown. Based on these results, VPHGs for astronomical instrumentation have been designed and manufactured.

OCIS codes: (160.5335) Photosensitive materials; (090.2890) Holographic optical elements; (090.7330) Volume gratings.

References and links

1. D. H. Close, "Holographic Optical Elements," Opt. Eng. **14**(5), 145402 (1975).
2. J. H. Burge, M. J. Fehniger, and G. C. Cole, "Demonstration of accuracy and flexibility of using CGH test plates for measuring aspheric surfaces," Proc. SPIE **3134**, 379–389 (1997).
3. C. Pruss, S. Reichelt, H. J. Tiziani, and W. Osten, "Computer-generated holograms in interferometric testing," Opt. Eng. **43**(11), 2534–2540 (2004).
4. G. Pariani, C. Bertarelli, G. Dassa, A. Bianco, and G. Zerbi, "Photochromic polyurethanes for rewritable CGHs in optical testing," Opt. Express **19**(5), 4536–4541 (2011).
5. D. G. Grier, "A revolution in optical manipulation," Nature **424**(6950), 810–816 (2003).
6. E. R. Dufresne, G. C. Spalding, M. T. Dearing, S. A. Sheets, and D. G. Grier, "Computer-generated holographic optical tweezer arrays," Rev. Sci. Instrum. **72**(3), 1810–1816 (2001).
7. D. R. Burnham and D. McGloin, "Holographic optical trapping of aerosol droplets," Opt. Express **14**(9), 4175–4181 (2006).
8. J. Liesener, M. Reicherter, T. Haist, and H. J. Tiziani, "Multi-functional optical tweezers using computer-generated holograms," Opt. Commun. **185**(1–3), 77–82 (2000).
9. S. Tay, P. A. Blanche, R. Voorakaranam, A. V. Tunç, W. Lin, S. Rokutanda, T. Gu, D. Flores, P. Wang, G. Li, P. St Hilaire, J. Thomas, R. A. Norwood, M. Yamamoto, and N. Peyghambarian, "An updatable holographic three-dimensional display," Nature **451**(7179), 694–698 (2008).
10. J. Geng, "Three-dimensional display technologies," Adv. Opt. Photonics **5**(4), 456–535 (2013).
11. I. K. Baldry, J. Bland-Hawthorn, and J. G. Robertson, "Volume phase holographic gratings: polarization properties and diffraction efficiency," Publ. Astron. Soc. Pac. **116**(819), 403–414 (2004).
12. P. A. Blanche, P. Gailly, S. Habraken, P. Lemaire, and C. Jamar, "Volume phase holographic gratings: large size and high diffraction efficiency," Opt. Eng. **43**(11), 2603–2612 (2004).
13. D. E. Battey, J. B. Slater, R. Wludyka, H. Owen, D. M. Pallister, and M. D. Morris, "Axial Transmissive f/1.8 Imaging Raman Spectrograph with Volume-Phase Holographic Filter and Grating," Appl. Spectrosc. **47**(11), 1913–1919 (1993).
14. L. W. Xiong, S. Liu, and B. X. Peng, "Mechanism of hologram formation in dichromated gelatin with x-ray photoelectron spectroscopy," Appl. Opt. **37**(17), 3678–3684 (1998).
15. J. R. Lawrence, F. T. O'Neill, and J. T. Sheridan, "Photopolymer holographic recording material," Optik (Stuttg.) **112**(10), 449–463 (2001).
16. A. Bianco, G. Pariani, A. Zanutta, and C. Bertarelli, "Materials for VPHGs: practical considerations in the case of astronomical instrumentation," Proc. SPIE **8450**, 84502W (2012).

#251864 Received 15 Oct 2015; revised 1 Dec 2015; accepted 8 Dec 2015; published 22 Dec 2015

17. F. K. Bruder, R. Hagen, T. Rölle, M. S. Weiser, and T. Fäcke, "From the surface to volume: Concepts for the next generation of optical-holographic data-storage materials," Angew. Chem. Int. Ed. Engl. **50**(20), 4552–4573 (2011).
18. M. Ortuno, E. Fernandez, R. Fuentes, S. Gallego, I. Pascual, and A. Belendez, "Improving the performance of PVA/AA photopolymers for holographic recording," Opt. Mater. **35**(3), 668–673 (2013).
19. R. Fernandez, S. Gallego, J. Frances, I. Pascual, and A. Belendez, "Characterization and comparison of different photopolymers for low spatial frequency recording," Opt. Mater. **44**, 18–24 (2015).
20. M. R. Gleeson and J. T. Sheridan, "A review of the modelling of free-radical photopolymerization in the formation of holographic gratings," J. Opt. A, Pure Appl. Opt. **11**(2), 024008 (2009).
21. M. R. Gleeson, J. Guo, and J. T. Sheridan, "Optimisation of photopolymers for holographic applications using the Non-local Photo-polymerization Driven Diffusion model," Opt. Express **19**(23), 22423–22436 (2011).
22. H. Li, Y. Qi, and J. T. Sheridan, "Three-dimensional extended nonlocal photopolymerization driven diffusion model. Part I. Absorption," J. Opt. Soc. Am. B **31**(11), 2638–2647 (2014).
23. H. Li, Y. Qi, and J. T. Sheridan, "Three-dimensional extended nonlocal photopolymerization driven diffusion model. Part II. Photopolymerization and model development," J. Opt. Soc. Am. B **31**(11), 2648–2656 (2014).
24. H. Kogelnik, "Coupled-wave theory for thick hologram gratings," Bell Syst. Tech. J. **48**(9), 2909–2947 (1969).
25. S. C. Barden, J. A. Arns, W. S. Colburn, and J. B. Williams, "Volume-phase holographic gratings and the efficiency of three simple volume-phase holographic gratings," Publ. Astron. Soc. Pac. **112**(772), 809–820 (2000).
26. M. G. Moharam and L. Young, "Criterion for Bragg and Raman-Nath diffraction regimes," Appl. Opt. **17**(11), 1757–1759 (1978).
27. F. Bruder and T. Fäcke, "Materials in optical data storage," Int. J. Mater. Res. **101**(2), 199–215 (2010).
28. H. Berneth, F. K. Bruder, T. Fäcke, R. Hagen, D. Hönel, D. Jurbergs, T. Rölle, and M.-S. Weiser, "Holographic recording aspects of high-resolution Bayfol HX photopolymer," Proc. SPIE **7957**, 79570H (2011).
29. H. Berneth, F.-K. Bruder, T. Fäcke, R. Hagen, D. Hönel, T. Rölle, G. Walze, and M.-S. Weiser, "Holographic recordings with high beam ratios on improved Bayfol HX photopolymer," Proc. SPIE **8776**, 877603 (2013).
30. L. Dhar, K. Curtis, and T. Fäcke, "Holographic data storage: Coming of age," Nat. Photonics **2**(7), 403–405 (2008).
31. F.-K. Bruder, F. Deuber, T. Fäcke, R. Hagen, D. Hoenel, D. Jurbergs, M. Kogure, T. Roelle, and M.-S. Weiser, "Full-Color Self-processing Holographic Photopolymers with High Sensitivity in Red - The First Class of Instant Holographic Photopolymers," J. Photopolym. Sci. Technol. **22**(2), 257–260 (2009).
32. F.-K. Bruder, F. Deuber, T. Fäcke, R. Hagen, D. Hoenel, D. Jurbergs, T. Roelle, and M.-S. Weiser, "Reaction-diffusion model applied to high resolution Bayfol HX photopolymer," Proc. SPIE **7619**, 76190I (2010).
33. R. Jallapuram, I. Naydenova, H. J. Byrne, S. Martin, R. Howard, and V. Toal, "Raman spectroscopy for the characterization of the polymerization rate in an acrylamide-based photopolymer," Appl. Opt. **47**(2), 206–212 (2008).
34. M. R. Gleeson, J. T. Sheridan, F.-K. Bruder, T. Rölle, H. Berneth, M.-S. Weiser, and T. Fäcke, "Comparison of a new self developing photopolymer with AA/PVA based photopolymer utilizing the NPDD model," Opt. Express **19**(27), 26325–26342 (2011).
35. F. Bruder, T. Fäcke, R. Hagen, D. Hönel, E. Orselli, C. Rewitz, T. Rölle, and G. Walze, "Diffractive optics with high Bragg selectivity: volume holographic optical elements in Bayfol HX photopolymer film," Proc. SPIE **9626**, 96260T (2015).
36. http://www.not.iac.es/instruments/alfosc/
37. J. Allington-Smith, "Spectroscopy," in *Optics in Astrophysics*, R. Foy, and F. C. Foy, eds. (Springer, 2005).

1. Introduction

Holographic optical elements (HOEs) are diffracting elements that modify an optical wavefront performing a specific action. Such kinds of elements have been known for a long time [1] and they have found applications in different fields. Indeed, they have been used extensively as Computer Generated Holograms (CGHs) in interferometric optical testing of aspheres or to align complex optical systems [2–4]. They have also found application as innovative optical tweezers [5–8] and in 3D displays [9, 10]. Among the different classes of HOEs, surely the volume phase holograms (vHOEs) are attractive especially for the peculiar properties in terms of diffraction efficiency. In these elements, a periodic modulation of the refractive index in a film of constant thickness is responsible for the diffraction of the light according to the refractive index pattern. In this category, Volume Phase Holographic Gratings (VPHGs) cover a relevant position as transmission dispersing elements in astronomical spectrographs [11, 12], Raman instrumentation [13] and in general in high efficient spectroscopic devices. In spectroscopy, they have to perform in terms of dispersion & resolving power, bandwidth and diffraction efficiency. This is even truer in the astronomical field where the requirements vary according to the different astronomical

#251864 Received 15 Oct 2015; revised 1 Dec 2015; accepted 8 Dec 2015; published 22 Dec 2015

scientific cases and sky targets. Indeed, each astronomical observation requires a particular dispersive element with a unique design in order to deliver the specific throughput, resolution and dispersion. The VPHG technology is interesting from this point of view, since each grating is a unique master grating, therefore the features can be tailored for matching the final performances.

One of the key issues in the development of VPHGs and more generally of volume phase HOEs is the photosensitive material. Indeed, up to now, the dichromated gelatin (DCG) is considered the reference material thanks to the large modulation of the refractive index that can be stored [14–16]. On the other hand, it requires a complex chemical developing process that, on one side, can be used to tune and adjust the final Δn, but on the other side prevents large scale and large size production. The possibility to have materials with similar performances but with self-developing properties is desirable, because they do not require any chemical post-process; moreover, the Δn formation can be monitored during the writing step. Photopolymers are probably the best alternative to DCG now, thanks to the improved features in terms of refractive index modulation, thickness control and dimension stability [15, 17–19]. Many studies have been carried out to understand deeply the behavior of this class of materials. Moreover, the formation of the refractive index modulation has been recently studied, especially by the research group of Sheridan [20–23], through the development of models that predict the trends as function of the material properties and writing conditions

A crucial point in the development of holographic materials suitable for VPHGs is the capability to tune finely the refractive index modulation of the material to match the design requirements and obtain high efficiency. In DCGs this is achieved by playing with the developing process. Therefore, it is necessary to find parameters for photopolymer recording that provide the same effect. In this work, after an introduction about the theory of VPHGs, the characterization of Bayfol HX photopolymers is reported showing the large possibility in tuning the refractive index modulation by changing the writing parameters. Finally, we report on the results we obtained in the design and manufacturing of VPHGs to be applied in ALFOSC, a low-resolution spectrograph for the Nordic Optical Telescope (NOT, Canary Islands).

2. VPHG: general theory and design guidelines

In a typical VPHG design, after having satisfied the dispersion and resolution requirements which fix parameters like the line density (Λ) of the grating, the incidence and diffraction angles, the design process moves to the optimization of the diffraction efficiency (both peak efficiency and bandwidth).

For this the main parameters to be considered are: i) the refractive index modulation Δn and ii) the film thickness d. Another parameter that can optimize the wavelength position of the efficiency curve is the slanting angle, i.e. the angle between the normal of the grating surface and the normal of the refractive index modulation plane.

Considering a sinusoidal refractive index modulation and working in the Bragg regime (the light is sent only in one diffraction order other than the zero), the well-known Kogelnik model can be used to understand the grating's behavior [24].

According to this model, the diffraction efficiency (η) of a transmission VPHG for unpolarized light at the Bragg angle (incidence angle α equal to the diffraction angle β) obeys to Eq. (1).

$$\eta = \frac{1}{2}\sin^2\left(\frac{\pi \Delta n d}{\lambda \cos \alpha_{2B}}\right) + \frac{1}{2}\sin^2\left(\frac{\pi \Delta n d}{\lambda \cos \alpha_{2B}}\cos(2\alpha_{2B})\right). \quad (1)$$

Here, Δn is the refractive index modulation of the material, d is the thickness of the film, λ is the wavelength and α_{2B} is the Bragg angle. For small angles, large diffraction efficiency is achieved when the product $\Delta n \times d$ is equal to half of the wavelength and this is the starting

#251864 Received 15 Oct 2015; revised 1 Dec 2015; accepted 8 Dec 2015; published 22 Dec 2015

point in the optimization process. As already stressed, not only the peak efficiency is important, but also the efficiency at the edges of the spectral range. According to the Kogelnik model, the spectral bandwidth of the diffraction efficiency curve is proportional to [25]:

$$\frac{\Delta\lambda}{\lambda} \propto \cot\frac{\alpha}{\Lambda d}. \tag{2}$$

In this equation, Λ is the line density of the grating and it is evident that the bandwidth is inversely proportional to Λ and the thickness of the grating. Therefore, the optimization of the diffraction efficiency curve, acting on the Δn and on d provides large differences in the grating response. If a grating works in the Bragg regime, the largest peak efficiency and bandwidth is obtained for very thin films and large Δn. Of course, the upper value of Δn is determined by the performances of the holographic material. In order to understand if a VPHG works in the Bragg regime, we have to refer to the parameter ρ [26]:

$$\rho = \frac{\lambda^2\Lambda^2}{n\Delta n}. \tag{3}$$

For values of ρ higher than 10, the grating is in the Bragg regime. High dispersion gratings (large Λ) usually work in this regime. Out this condition, the VPHG works in the Raman-Nath regime [26] and it diffracts the light with a non-negligible efficiency in more than one diffraction order. In this case, the diffracted energy is of the order of $1/\rho^2$, which means proportional to $(1/\Lambda)^4$ and to Δn^2. Consequently, for low dispersion gratings, it is better to increase the film thickness and reduce the Δn in order to have both: large peak efficiency and bandwidth. The smaller the Λ parameter, the smaller the required Δn and larger d; Fig. 1 reports two examples for explaining this trend, namely the diffraction efficiency of two VPHGs with 2000 l/mm and 500 l/mm calculated at the Bragg angle at 0.5 μm by means of Rigorous Couple Wave Analysis (RCWA) approach.

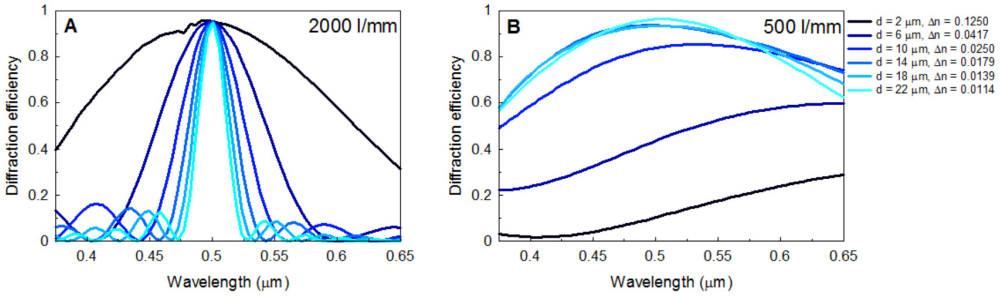

Fig. 1. Simulations of diffraction efficiency, for unpolarized light, of VPHGs with 2000 l/mm (A) and 500 l/mm (B) as function of d – Δn couples. The incidence angle is the Bragg angle at 0.5 μm.

Moreover, a VPHG working at higher wavelengths requires larger values of Δn and/or d to achieve the same efficiency performances, both if it works in the Raman-Nath and Bragg regimes. Figure 2 summarizes these guidelines.

#251864 Received 15 Oct 2015; revised 1 Dec 2015; accepted 8 Dec 2015; published 22 Dec 2015

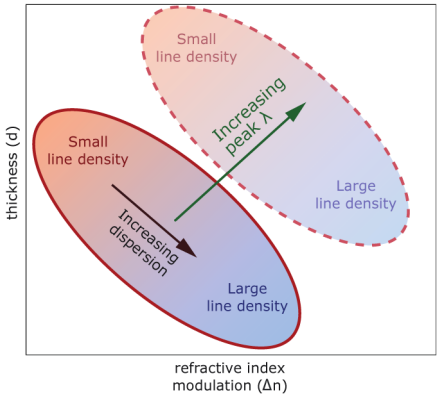

Fig. 2. Scheme reporting the rules for designing high efficient and wideband VPHGs in the *d* – *Δn* space.

From the point of view of holographic materials, we can state that for low Λ VPHGs, the main issue is the manufacturing of thick holographic films preserving the optical quality and providing a uniform thickness, but at the same time addressing the *Δn* to a well-defined value. On the opposite, for high Λ VPHGs, the main issue is to push the *Δn* as high as possible and to make very thin film with constant thickness. Of course, for intermediate conditions, a fine-tuning of *d* and *Δn* is necessary to reach the desired performances.

A holographic material suitable for the manufacturing of high performances VPHGs should show a tunable modulation of the refractive index together with a wide range of thicknesses. Moreover, the tuning of the *Δn* should be as simple and reliable as possible.

3. Photopolymeric material characterization and results

The newly [27–29] developed photopolymer film technology (Bayfol HX film) evolved from efforts in holographic data storage (HDS) [27, 30] where any form of post processing is unacceptable. These new instant developing recording media open up new opportunities to create vHOEs for new diffractive optics and have proven to be able to record predictable and reproducible optical properties. This was demonstrated recently also for transmission holograms and directional diffusors [28, 31].

Bayfol HX represents a technology platform of customized holographic recording films. Depending on the application requirements, the substrate can be varied toward characteristics like thickness, (low) birefringence and optical flatness. The photopolymer layer can be designed towards e.g. (high or low) index modulation, transparency, wavelength sensitivity (monochromatic or RGB) and required thickness to match the gratings wavelength and/or angular selectivity.

The Bayfol HX films consist of a three-layer stack: a substrate, a light-sensitive photopolymer and a protective cover film. The protective cover film can be removed so the photopolymer film can be index matched by simply laminating it on glass plates.

Among this family, we initially characterized a research level sample having a nominal thickness of 16 µm, RGB sensitive, coated onto a polyamide substrate 60 µm thick.

3.1 Spectral characterization

In order to understand the usable spectral range of Bayfol HX material, we recorded the transmission spectrum from 200 to 2500 nm, before and after the light exposure using an unfiltered halogen lamp with a fluence of ~50 J/cm^2 (Fig. 3). The behavior in the NIR spectral region is dominated by the polymer substrate. Indeed, the material is transparent up to 2.2 µm, where the infrared overtones of the polyamide start to absorb strongly. It seems that no evident absorptions come from the photopolymer system. In the UV region, the photopolymer

#251864 Received 15 Oct 2015; revised 1 Dec 2015; accepted 8 Dec 2015; published 22 Dec 2015

shows a steep transition opaque to transparent at 312 nm. Moreover, in the unexposed film, we clearly identify the absorption peaks of the sensitizers that make the material panchromatic. After the bleaching step, some weak residual absorption bands are present in the visible. In general, higher residual absorption occurs for thicker films and this is especially true approaching the UV cut-off. Therefore, a particular attention must be paid to VPHGs working in the UVA, where the absorption could reduce the final diffraction efficiency.

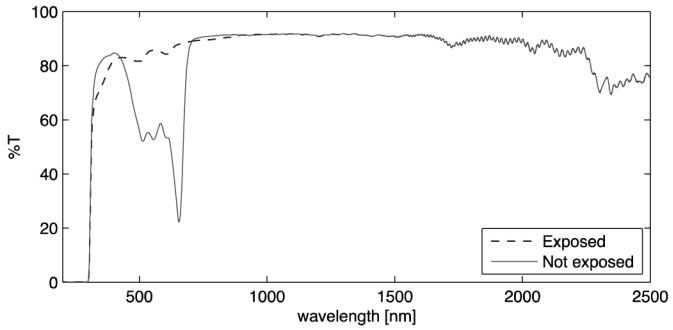

Fig. 3. UV-vis-NIR spectra of the RGB Bayfol HX (16 μm) photopolymeric material before (solid line) and after photo-bleaching (dashed line).

3.2 Tunability: Δn as function of power density

The most convenient propriety of a holographic material for VPHGs is for sure the ability to tune properly the refractive index modulation, in order to assess the spectral requirements that have been defined in the design phase.

The Bayfol HX photopolymeric material generates the index difference through a reaction-diffusion mechanism, which involves a competing process between the migration of the monomers inside the film and the polymerization of the material itself [32]. The photopolymerization occurs in the exposed regions of the pattern (constructive interference), while due to a concentration gradient, the monomers migrate from the dark to the exposed regions being polymerized themselves.

The photopolymerization of this system depends upon the writing power density [33]. With increasing the writing power, the monomer conversion occurs more and more also in the dark fringes. The maximum achievable index modulation starts to drop.

Figure 4 reports the values of Δn as function of the writing power density ranging from 0.143 to 21.5 mW/cm^2 (these intensities are the measurements of one of the two identical beams) for samples with increasing line density (600, 1000, 1400 l/mm). The total illumination dose was kept constant at 42 mJ/cm^2, therefore the exposure time for each sample changed according to the laser power. With this dose, we were sure to reach the plateau value of the refractive index modulation during the writing step.

Similar gratings written with different power, result in different final refractive index modulation. The decreasing trend with the power density is clear for all the line densities explored. It is important to point out the relatively large values of Δn (in between 0.03 and 0.04) that can be achieved in transmission vHOEs by using Bayfol materials, especially if we consider the family of photopolymers.

#251864 Received 15 Oct 2015; revised 1 Dec 2015; accepted 8 Dec 2015; published 22 Dec 2015

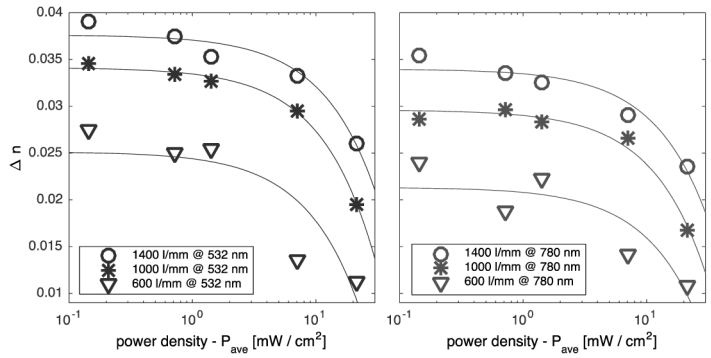

Fig. 4. *Δn* as function of the mean value of the intensity of the two writing arms. The total dose was kept constant at 42 mJ/cm^2 (referred to double beam writing process). Continuous lines are a linear fit of the data.

Another peculiar effect is the dependence of *Δn* on the line density: the curves of samples with higher line densities are shifted at larger *Δn* values. This effect is again easily understandable if we think at the reaction-diffusion mechanism of the photopolymer. Increasing Λ means a shorter path to travel for the monomer, thus a facilitated process of *Δn* formation. This is true in the range of line density here considered, for much higher Λ, a *Δn* cut-off could occur because of the nonlocal effects [21]. It is important to notice that Bayfol HX photopolymers showed a much smaller nonlocal response parameter, which turns into a larger resolution in comparison with standard AA/PVA photopolymers [34].

We also notice a dependence of the *Δn* with the reconstructing wavelength. This can be ascribed to the dispersion of the refractive index with the light frequency; indeed, by increasing the frequency, the refractive index increases (normal dispersion). Such increment is different for the exposed and unexposed regions because of the different polarizability. In particular, we could expect a more pronounced rise of refractive index for the exposed regions, with a consequent growth of *Δn* for shorter wavelengths, as experimentally verified. Moreover, the amount of change is compatible with the chemical composition of the photopolymer system.

From these results, it is evident how with this material we can achieve precise *Δn* values in accordance with the design goals, in a range strictly related to the lines per millimeter of the target VPHG. For example, if we need a diffraction grating with 1400 l/mm and we can deal with powers from 0.143 to 21.5 mW/cm^2, the achievable *Δn* can be from 0.026 to 0.039.

3.3 Tunability: Δn as function of beam ratio intensity

The second strategy for the tuning of the *Δn* is related to the intensity ratio of the two writing beams. It is well known that in order to obtain the largest contrast in the interference pattern, the intensity of the two laser beams must be as equal as possible. Only in this condition, the intensity in the minima of the sinusoidal pattern is zero. This is for sure the best achievable condition for maximizing the refractive index modulation while, if lower *Δn* values have to be achieved, unbalanced writing intensities can be used.

The unbalanced beam ratio will result, in fact, in a smaller amplitude sinusoidal pattern with an average values > 0, which is proportional to the intensity ratio. The effect is a concomitant polymerization even in these areas, counteracting the monomers migration.

In order to evaluate the extent of this behavior, we performed writings at different ratios, while maintaining constant the total irradiation dose at 42.8 mJ/cm^2. Moreover, we decided to keep fixed the intensity of the second writing beam P2 = 1.43 mW/cm^2 and vary the intensity of P1 from 0.143 to 2.86 mW/cm^2, so that the ratios P1/P2 are 1:10, 1:2, 1:1, 1.5:1, 2:1.

The typical trend of the *Δn* with the fluence (or exposure time) is an increasing curve with a plateau value which is inversely proportional to the writing power density [34]. During the

#251864 Received 15 Oct 2015; revised 1 Dec 2015; accepted 8 Dec 2015; published 22 Dec 2015

exposures we monitored the grating's *Δn* formation to ensure that the plateau was reached with the provided fluence, therefore the maximum *Δn* value for that particular writing power.

As can be seen in Fig. 5, a strong dependence of the *Δn* with the intensity ratio occurs, confirming that the best condition for the recoding of transmission VPHGs is the balanced (50:50) beam ratio, but lower values can be addressed precisely when different ratios are set. This strategy is especially useful when very low *Δn* values are required and high values of laser power cannot be provided to constrain the *Δn* with the balanced beams.

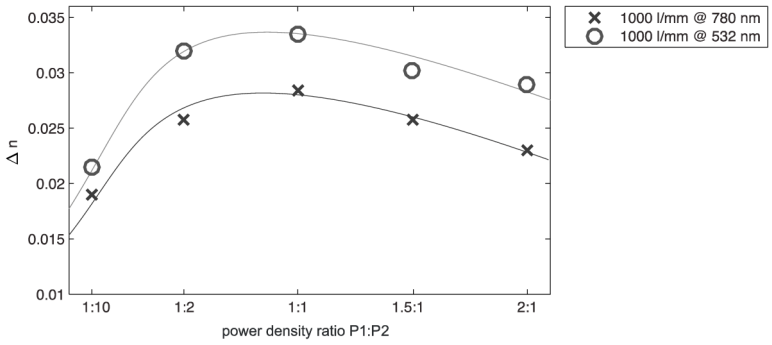

Fig. 5. *Δn* as function of the ratio between the power of two writing beams P1 and P2 for a 1000 l/mm grating. The dose was kept constant at 42.8 mJ/cm^2 (referred to double beam writing process).

Another possibility for tuning the *Δn* could be a pre-exposure that is able to partially consume the monomers in the holographic film. Moreover, the pre-exposure can be used to depleting the oxygen dissolved in the photopolymeric layer, which is an inhibitor of the photoreaction [35].

5. Practical case: optimization of dispersive elements for an astronomical spectrograph

Based on the aforementioned features of Bayfol HX photopolymers, it is important to show a practical case, where these materials have been used and where the dispersing devices can be integrated in a working spectrograph.

We focused the attention to the dispersing elements of ALFOSC (The Andalucia Faint Object Spectrograph and Camera) mounted on the Nordic Optical Telescope (2.56 meters, La Palma, Spain) [36]. This instrument is a focal reducer providing low resolution spectra and it is based on GRISM dispersing elements (a grating coupled with prisms) [37].

Recently, there was the interest to develop some VPHGs with a resolution of about 1100 that can cover the blue and green wavelength range, with an improved efficiency in comparison to the actual dispersing elements based on ruled gratings. The requirements about these gratings are reported in the Table 1.

Table 1. NOT's GRISMs main specifications: (1) Central wavelength of the grating; (2) Linear dispersion of the grating; (3) Resolution, R = λ/Δλ; (4) Wavelength range; (5) minimum 1-st order diffraction efficiency at the peak wavelength; (6) minimum 1-st order diffraction efficiency at the wavelength range edges.

Device name	*Central λ [nm] (1)*	*Dispersion [Å/px] (2)*	*Resolution (3)*	*Δλ [nm] (4)*	*Min. peak η (5)*	*Min. side η (6)*
BLUE	430	0.9	1100	337 – 532	80%	30%
GREEN	565	1.2	1100	443 – 687	80%	30%

5.1 Design of the VPHGs

The first step of the design process was the calculation of the grating's line density Λ and incidence angle α to achieve the spectral requirements. After the design of the VPHGs in

#251864 Received 15 Oct 2015; revised 1 Dec 2015; accepted 8 Dec 2015; published 22 Dec 2015

terms of spectral proprieties, RCWA simulations have been performed to find the material properties (*d* and *Δn*) that maximize the diffraction efficiency in the spectral range of interest.

Regarding the material's thickness, a preliminary optimization induced the selection of a custom Bayfol HX films of 10 μm. Since the thickness parameter was set, the optimization of the diffraction efficiency was carried out acting on the *Δn*, while maintaining fixed the line density Λ (1080 l/mm for the BLUE and 820 l/mm for the GREEN) and the incidence angle α (13.4° in air for both gratings). The calculated diffraction efficiency curves (for unpolarized light) are reported in Fig. 6. We notice the large change in diffraction efficiency with small changes in *Δn*. The goal of the optimization process was not only to reach a high peak efficiency, but also to have enough signal at the edges of the spectral range, in particular it was necessary to enhance the efficiency at the low wavelength edge for both gratings.

In order to reach the target *Δn* values during the production process, we had to tune properly the writing power density according to the methodology described in the previous sections.

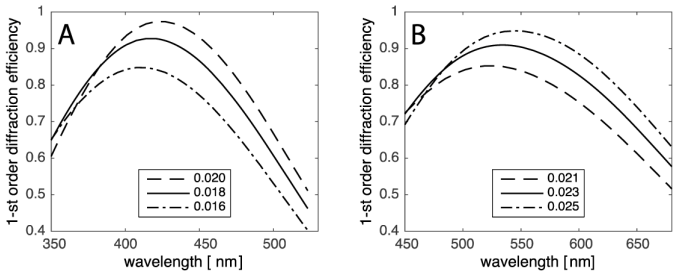

Fig. 6. RCWA simulations with different refractive index modulation values (reported in the legend) for a 10 μm thick grating and an incidence angle of 13.4°. A) Wavelength range for the BLUE device (1080 l/mm); B) wavelength range for the GREEN device (820 l/mm).

5.2 Manufacturing and testing

The grating manufacturing started with the adjustment of the holographic setup to provide the desired line density. Then, the optimization of the laser power density was performed in order to achieve the target *Δn* for the specific lines/mm.

After the optimization phase we recorded the VPHGs using the same material but with the following laser power density for each grating: the BLUE (1080 l/mm) with P_{ave} = 19.3mW/cm^2, and the GREEN (820 l/mm) with P_{ave} = 4.3 mW/cm^2. After the production of the two gratings we measured the efficiency of the 1st diffracted order at different wavelengths, with the purpose to verify, after the fit of the acquired data, the *Δn* achieved. As displayed in Fig. 7, the RCWA fits confirmed the correct *Δn* achieved for each grating.

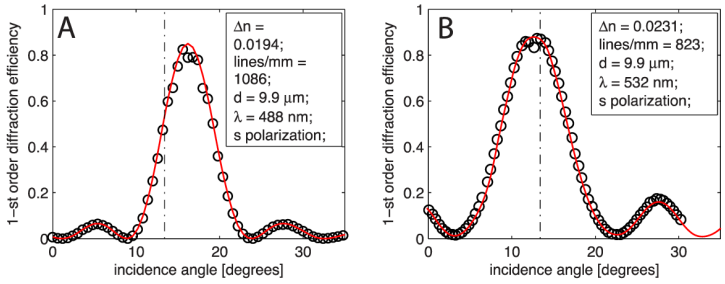

Fig. 7. Efficiency measurements at fixed wavelength (s-polarized), fitted with RCWA, for the two VPHGs composing the GRISMs for the spectrograph ALFOSC; A) is the BLUE grating, B) is the GREEN grating. Inside the inlets are reported the calculated values of refractive index modulation. The vertical dotted lines indicate the angle at which the gratings work in the GRISM configuration. The light is deviated by the prisms and enters the VPHGs at 13.4°.

#251864 Received 15 Oct 2015; revised 1 Dec 2015; accepted 8 Dec 2015; published 22 Dec 2015

We have then assembled the GRISMs and measured their diffraction efficiency. Figure 8 reports the diffraction efficiency curves of the two GRISMs constructed by joining singular wavelength measurements. The values were collected measuring the intensity of the diffracted beam after passing through the assembled devices at the normal incidence (so in the working condition of the device). We highlighted the trend with a polynomial fit that shows a peak diffraction efficiency above 80% for the two GRISMs, matching the requirements. So large efficiencies indicate also that the reflection losses in the GRISM assembly prism/VPHG/prism were minimized.

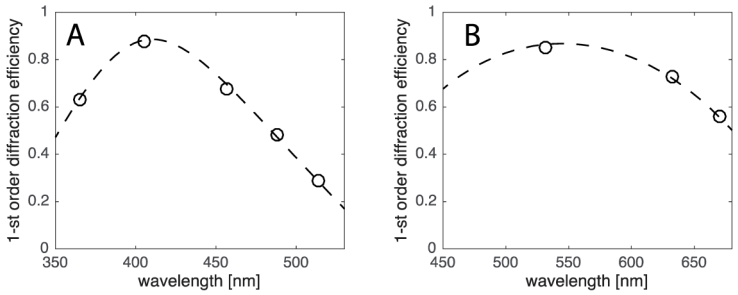

Fig. 8. Diffraction efficiency measurements (unpolarized light) and fit of the data of the two complete NOT devices; A) is the BLUE grism, B) is the GREEN grism.

Thanks to these positive evidences at the laboratory level, we delivered the GRISMs for the integration inside the spectrograph. Table 2 gathers all the proprieties of the new GRISMs installed at NOT and Fig. 9 reports a picture of the two devices right before the shipping to the NOT for the integration.

Table 2. NOT's delivered GRISMs main specifications summary: (1) Working central wavelength of the grating; (2) pixel dispersion of the grating; (3) Wavelength range; (4) Resolution, R = λ/Δλ; (5) pitch of the grating; (6) final refractive index modulation of the grating.

Device name	*Central λ [nm] (1)*	*Dispersion [Å/px] (2)*	*Δλ [nm] (3)*	*R (4)*	*l/mm (5)*	*Δn (6)*
BLUE	430	0.918	337 - 523	1129	1086	0.019
GREEN	562	1.212	443 - 687	1110	823	0.023

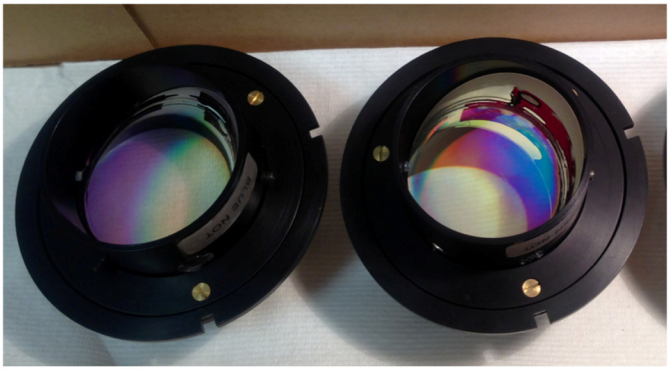

Fig. 9. Photo of the two dispersive elements in their housing ready to be mounted into the spectrograph.

For retrieving the quantitative throughput of the newly installed devices, we decided to compare them with old GRISMs based on ruled gratings, which possess similar characteristics and were already mounted in the spectrograph.

#251864 Received 15 Oct 2015; revised 1 Dec 2015; accepted 8 Dec 2015; published 22 Dec 2015

The comparison was performed observing the spectra of photometric-standard stars SP0644 + 375 and SP0305 + 261. This object class is a well-known series of stars that have had their light output already measured very carefully determining their stable exact brightness.

In Fig. 10, we report the calibrated and reduced spectra (with conventional IRAF procedure) acquired using the different gratings with identical exposure times. From these spectra, the effective gain in efficiency can be evaluated. In the figure, the total system efficiency curves are the convolution of the efficiency curves of the gratings with the efficiency of the telescope (mirrors and all the other components) and the spectral magnitude of the observed star.

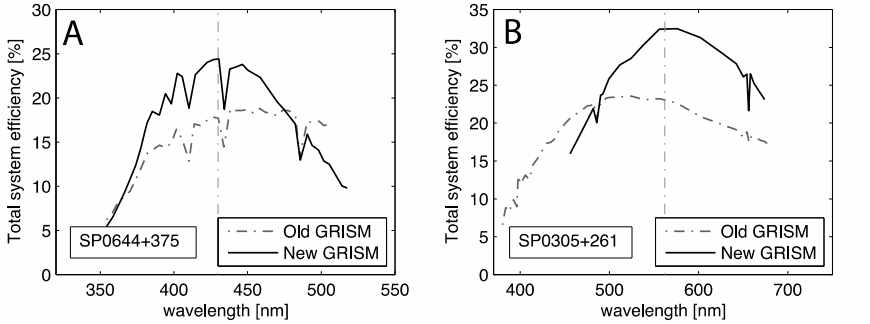

Fig. 10. Comparison of photometric-standard stars' spectra. Total system throughput of the NOT telescope with BLUE (A) and GREEN (B) VPHG devices and with already mounted dispersive elements (Grism 7 and Grism 16).

As evidenced by the spectra, for all the delivered devices, the on-sky results are in good accordance with the laboratory measurements (position of the peak and bandwidth).

With the realization of these devices, we were able to address the targeted astronomical requirements with a substantial increase in system throughput. This means that we were able to reach the same signal-to-noise ratio with lesser time than the exposure with the old telescope's devices, advantage that is very significant since nowadays the typical time scales for an observation are in the order of hours.

6. Materials and methods

6.1 Holographic writing set-up and VPHG manufacturing

The VPHGs' writing process is performed using a DPSS laser (Torus, Laser Quantum, 500 mW single mode TEM00) at 532 nm, integrated onto an isolated optical table. The gratings were written with a standard two-beams holographic setup: it consists in a 50:50 beam splitter that separates the initial laser beam, neutral density filters to homogenize and dim the power, spatial filters to clean out the beams, two ϕ100 mm collimating doublets and plane λ/10 mirrors mounted on rotating stages. The angle defined by the tilt of the two mirrors selects the lines per millimeter that are transferred onto the photosensitive film. After the holographic exposure a fixation process with a halogen lamp is necessary in order to complete the polymerization even in the unexposed regions of the grating and to bleach the dye left. The samples were post-exposed for 30 minutes with a 20W halogen lamp at a distance of 10 cm (~28 mW/cm^2).

6.2 Characterization of VPHGs

The diffraction efficiency of VPHGs was measured using different laser sources, from 405 nm to 1064 nm. The use of laser lines instead of a polychromatic light source makes the application of grating's models (Kogelnik, RCWA) easier, reducing the source of errors. For

#251864 Received 15 Oct 2015; revised 1 Dec 2015; accepted 8 Dec 2015; published 22 Dec 2015

the same reason, the laser light, before hitting the sample, is firstly depolarized and then polarized again. The raw diffraction efficiency is calculated measuring the intensity of the diffracted order of interest, in comparison to the light intensity without the grating. The grating under test is placed on the sample holder, which is in turn mounted on a rotating stage. In this way, the incidence angle is set. The diffracted light (according to the grating's equation) is measured by a Si photodiode, mounted on a second motorized rotating stage. Such raw diffraction efficiency comprises the reflection losses (no AR coating was present onto the surfaces) and the absorption losses (residual absorption of the holographic material). Since the models we used to have the estimation of the material's properties (Δn and thickness) provide the intrinsic efficiency of the VPHG, we applied the corrections, for both reflection and absorption losses, to the experimental efficiencies in order to make a reliable fitting possible. Regarding the reflection losses, the approach is to apply the classical Fresnel equations as function of the α and β angles to the interface substrate/air. In other words, we neglect the reflection losses between the holographic material and the substrate, since they are much smaller than the losses between the substrate and the air. As for the absorption component, it is extrapolated from the UV-Vis spectrum of the photosensitive material, which is then corrected for the effective thickness during the efficiency measurement.

The UV-VIS-NIR spectra were collected with a Jasco V570 spectrometer. The RCWA code was written in C by Gary Bernstein and then implemented in Matlab.

7. Conclusions

The performances of volume phase holographic elements depend on the photosensitive material. In particular, the diffraction efficiency is governed by the refractive index modulation (Δn) and film thickness. Bayfol HX photopolymer film is a new class of self-developing photosensitive materials that show interesting properties in terms of Δn and more important on control of the index modulation. We showed how it is possible to tune the Δn by changing the writing power density and/or the intensity balance of the two laser beams.

An index modulation Δn of the order of 0.035 can be achieved and a tuning in between 0.01 and 0.037 is possible. Such values are large in the field of holographic materials and make the realization of high efficient volume phase holograms possible together with a wide bandwidth. In order to prove the suitability of Bayfol HX for astronomical applications, we have designed and manufactured VPHGs using several versions of this material. The efficiency has been measured and turned to be larger than 80%. The performances have been evaluated in field trials providing an increase in overall instrument's efficiency on the order of 40% with respect to dispersing elements based on ruled gratings.

The precision reached with the production of these astronomical devices was satisfactory in terms of dispersion proprieties, which is the most stringent parameter in the design of an astronomical VPHG. Besides, the accuracy of the Δn addressing was more than adequate for matching all the efficiency requirements of the ALFOSC astronomical spectrograph.

Acknowledgment

This work was partly supported by the European Community (FP7) through the OPTICON project (Optical Infrared Co-ordination Network for astronomy) and by the INAF through the TECNO-INAF 2014 "Innovative tools for high resolution and infrared spectroscopy based on non-standard volume phase holographic gratings".

We would like to thank Dr. John Telting and all the staff of the Nordic Optical Telescope for the fruitful collaboration and for the support in the acquisition and reduction of the astronomical data used in this paper.

#251864 Received 15 Oct 2015; revised 1 Dec 2015; accepted 8 Dec 2015; published 22 Dec 2015